WILEY-VCH

DOI: 10.1002/ ((please add manuscript number))
Article type: Full Paper

Plasmon-Promoted Electrochemical Oxygen Evolution Catalysis from Gold Decorated MnO_2 Nanosheets under Green Light

Jing Xu, Peng Gu, David J. S. Birch and Yu Chen**

Department of Chemistry, Fudan University, 2005 Songhu Road, Yangpu District, Shanghai 200438, P. R. China
E-mail: tommy861007@hotmail.com
Photophysics Group, Department of Physics, SUPA, University of Strathclyde, 107 Rottenrow, Glasgow G4 0NG, UK
E-mail: y.chen@strath.ac.uk
School of Chemistry and Chemical Engineering, Yangzhou University, 180 Siwangting Road, Yangzhou, Jiangsu Province 225002, P.R. China

Keywords: surface plasmon resonance, catalysis, hybrid materials, gold nanoparticles, charge transport

The oxygen evolution reaction (OER) is of great importance for renewable energy conversion and storage, however, the intrinsic process is sluggish and suffers from severe efficiency loss as well as large over-potentials. In this work, with the introduction of the plasmonic effects by design of the Au-MnO_2 hybrid catalysts, we demonstrate that this photophysical phenomenon could largely promote the confinement of the outer electrons of Mn cations by plasmonic "hot holes" generated on gold surface. These "hot holes" work as the effective electron trapper to form the active Mn^{n+} species which could provide active sites to extract electrons from OH^- and eventually facilitate the electrochemical OER catalysis under low laser power. By tuning the laser intensity from 100 to 200 mW, the over-potential is decreased from 0.38 to 0.32 V, which is comparable to IrO_2 and RuO_2 catalysts. These findings may provide insights into activation of plasmon-promoted electrocatalysis under low power laser irradiation/treatment and the design of novel composite electrocatalysts.

1. Introduction

Advanced materials in efficient harvesting, storage and utilization of renewable energy are of great importance in current energy research.[1–6] The splitting of water either by electricity-driven or photo-driven has been widely studied for energy conversion into fuels and chemicals; in particular, the oxygen evolution reaction (OER) plays a vital role by giving protons and electrons to these processes.[7–11] However, the intrinsic process of OER is sluggish and suffers from severe efficiency loss as well as large over-potentials.[12,13] Therefore, finding proper OER catalysts is critical in accelerating the reaction, reducing the over-potential and improving the overall efficiency. In the past few years, transition-metal based materials (such as cobalt oxides and nickel oxides) have been applied as OER catalysts under alkaline and neutral conditions for the benefits of cost effectiveness, good stability and low pollution.[14–16] It is believed that the transition-metal ions in materials undergo progressive oxidation to higher valence states or electron confinement prior to the OER, during the electrochemical process.[16–19] This indicates that the highly oxidative metal ions may be the active sites of OER catalysts. The corresponding investigations confirm that the OER catalytic performance may depend on the outer electron states of the transition-metal species.[20]

Localized surface plasmon resonance (LSPR) is the coherent charge density oscillation, usually in a noble metal (such as gold and silver) nanostructures, which is excited by the electromagnetic irradiation (light).[21,22] This optical phenomenon attracts a great deal of attention, because it is capable of efficiently absorbing photons and converting light energy to hot electrons (also referred to “energetic electrons”) and enhanced local electric field.[23–26] During the LSPR process, hot electrons will be excited and transferred, and simultaneously leading to the hole generation on the surface of plasmonic materials to capture external electrons.[24] Meanwhile, the local electric field of the plasmonic nanostructures could be

greatly enhanced, which leads to many unique features such as plasmon enhanced fluorescence and SPASERs.[27,28] Such a LSPR effect enables the efficient energy harvest and conversion for photovoltaics and photo-driven water splitting.[23,29] Inspired by the above phenomena, hybridizing the transition-metal catalyst with plasmonic metal nanoparticles would cause electron-transition metal species, and eventually promote the OER catalytic performance. Thus, the investigation of transition metal species with plasmonic nanoparticle hybrids is highly necessary. In late 2016, Ye' group, for the first time, proposed a $Ni(OH)_2$-gold catalyst for OER and showed good catalytic performance under intense 1 W of 532 nm laser.[30] However, the study of plasmon-assisted electrocatalytic OER behaviours is still in its early stage, and few reports have come into view on the coupling effects of high-performance OER catalysis.[31,32]

In this study, the gold decorated two-dimensional (2D) δ-MnO_2 nanosheet composites were successfully prepared with various percentage of gold loading. The composite showed excellent OER catalytic performance under and after green laser excitation. In this composite, δ-MnO_2 nanosheets were chosen as the primary OER catalysts for the unique 2D structures and good electrochemical performance. Gold nanospheres (GNSs, 12.9 nm in radius) were decorated on the 2D MnO_2 nanosheets as the nanoantennas and plasmonic exciters. Importantly, low power of 100 and 200 mW coherent 532 nm lasers were used to perform the experiments rather than 1 W intense laser used in previous studies. The electrochemical results showed that the OER catalytic performance could be severely enhanced by activating the LSPR from GNSs under the 532 nm laser irradiation. Interestingly, after the laser treatment under a dark environment, the composite maintained OER catalysis performance with an over-potential of 0.32 V. Our study indicates that plasmon-induced hot-electron excitation could largely promote the confinement of the outer electrons within transition-metal species. The plasmonic "hot holes" nearby may work as effective electron traps to form active Mn^{n+} species that could provide active sites to extract electrons from OH^- and finally enable high-efficiency electrochemical water oxidation at lower onset potential. These findings may provide insights on activation of

plasmon-induced electrocatalysis under low power laser irradiation/treatment and the design of novel composite electrocatalysts.

2. Results and Discussion

GNSs with an average diameter of 12.9 nm were first prepared by reduction of $HAuCl_4$ with CTAB as shown in Figure S1 [Supporting Information (SI)].[22,33] Then, ultrathin δ-MnO_2 nanosheets were synthesized via a modified distillation reflux method (see in Figure S2, SI).[34] Based on the opposite surface charge of the MnO_2 nanosheets (ζ-potential = - 41.3 mV) and the GNSs (ζ-potential = 33.8 mV) on show in Figure S4 [SI], they could be physically assembled through the electrostatic interaction in the solution, which finally result in the formation of Au-MnO_2 nanocomposites.[34] **Figure 1**a-c are the scanning electron microscopy (SEM) and transmission electron microscopy (TEM) images in-between GNSs and MnO_2 nanosheets, respectively. It is clear that the GNSs were well dispersed on the surface on MnO_2 nanosheets. The high-resolution TEM (HRTEM) image displayed in Figure 1d shows the lattice fringe between GNS and MnO_2 nanosheet and confirms the close interfacial contact which would support the "hot electron" transfer.[35] Figure S3 [SI] shows HRTEM images of δ-MnO_2 with an ~3 nm thickness, indicating the ultrathin 2D nanostructures. The inset, Figure 1e, shows the selected area electron diffraction (SAED) image of the GNS on MnO_2 nanosheet in Figure 1d, in which the diffraction rings correspond to the (111), (200) and (222) reflections of the face-centred cubic (fcc) gold nanosphere. Figure 1f shows the dark-field scanning transmission electron microscopy (STEM) image of a giant piece of Au-MnO_2 nanocomposite. The corresponding elemental mappings are on shown in Figure 1g-j, from which the uniform distribution of GNSs over MnO_2 nanosheets is further confirmed.

Figure 2a shows the corresponding X-ray diffraction (XRD) pattern of Au-MnO_2 nanocomposites and bare MnO_2 nanosheets. Consistent with the SEM and TEM images, both

the δ-MnO_2 (JCPDS 42-1317) and cubic gold (JCPDC 01-089-3697) are recognized. The peaks at 2-thetas of 12.2°, 24.5°, 37.1° and 66.2° reflects the (001), (002), (200) and (310) planes of δ-MnO_2 nanosheets, respectively; and the 37.5°, 44.9° and 77.9° reflects the (111), (200) and (220) planes of the fcc gold, which is also matched with the SAED pattern in Figure 1d.[34] Importantly, the unusual intensity at 37.1° comparing to the standard may be caused by coating sample on a glass substrate for XRD measurement, which leads to the over exposure of (200) plane of δ-MnO_2 nanosheets. The absorption properties of GNSs, δ-MnO_2 nanosheets and Au-MnO_2 nanocomposites were investigated via a UV-vis spectrophotometer. After assembled the GNSs on δ-MnO_2 nanosheets, the extinction spectra of Au-MnO_2 nanocomposites exhibits an absorption peak at 525 nm, as shown in Figure 2b. In addition, with the increase of gold loading the plasmon absorption peak is getting stronger. Meanwhile, the peak wavelength of Au-MnO_2 nanocomposites is slightly red-shifted comparing to the pure GNSs (inset of Figure 2b), which indicates the electronic interaction between gold and MnO_2, and proves the successful assembly of Au-MnO_2 nanocomposites, eventually.[31]

The standard and plasmon-promoted electrocatalytic performance of Au-MnO_2 nanocomposites towards oxygen evolution reaction were studied in O_2-saturated 0.1 M KOH electrolyte at room temperature via a typical three-electrode system. Meanwhile, GNSs and δ-MnO_2 nanosheets were also tested as references under identical conditions. A 532 nm laser source was applied corresponding to maximum LSPR peak of GNRs. **Figure 3**a shows the OER polarization (linear sweep voltammetry, LSV) curves of δ-MnO_2 nanosheets and Au-MnO_2 nanocomposites, with and without laser irradiation (100 and 200 mW of 532 nm green laser), at a scan rate of 5 mV/s. Without gold, the δ-MnO_2 nanosheets exhibit much weaker OER electrocatalytic performance under dark and 100 mW laser irradiation. Although the Au-MnO_2 nanocomposites do not show an obviously enhanced catalytic performance compared to δ-MnO_2 nanosheets in a dark environment, they show a much smaller over-potential at 0.38 and

0.32 V (vs reversible hydrogen electrode, RHE) once the surface plasmon resonance is excited by the 100 and 200 mW of 532 nm laser, respectively. In addition, Figure 3d shows the negligible OER catalytic performance of GNSs in a dark environment and under 532 nm laser irradiation. Meanwhile, to identify the wavelength dependence properties, a 200 mW of 650 nm laser was used to carry out the same experiment. As shown in Figure S6 [SI], Au-MnO_2 nanocomposite catalysts show a negligible current enhancement under the 650 nm laser irradiation, where a slight change in current density may be caused by the photothermal effect and broad band of plasmon peak.[36] These results clearly show that such an active photo-enhancement effect is mainly caused by the gold LSPR excitation.

To further investigate this photo-enhancement effect, varying amounts of gold loading were carried out. The loading concentration of gold is from 0 to 8.3 wt % and the obtained samples were denoted as L0-L4 and A0-A4, which were performed for the catalytic experiments under and after laser irradiation, respectively. It can be seen in Figure 3b that the electrocatalytic performance of the "as-prepared" samples under 100 mW laser irradiation improves progressively as the increase of GNSs loading, where the L4 (maximum gold loading) shows a reasonable OER over-potential at 0.38 V. Additionally, Figure 3c exhibits the LSV curves of the "as-prepared" samples under more intense 200 mW laser irradiation. Showing the similar performance trend as Figure 3b, the OER over-potential of L4 is further reduced to 0.32 V. This performance is much better than that of Au-MnO_2 nanocomposites under a dark environment and comparable with IrO_2 and RuO_2 catalysts, which indicates that the efficient electrocatalytic OER reaction could be realized under light irradiation by grafting plasmonic antennas on conventional transition metal oxides. Interestingly, the samples maintained the OER catalytic performance after 5-min treatment of 200 mw laser irradiation. As shown in Figure 3d, the OER over-potential of A4 is maintained at around 0.32 V, which is at the same level of L4 under 200 mW laser irradiation. Tafel slope analyses were also performed to analyse the kinetics of OER in this work, as shown in Figure 3f. With laser power increased from 100 to 200 mW, the Tafel

slope is decreased from 91 to 68 mV/dec, which clearly indicates that the kinetics of oxygen evolution reaction are facilitated by LSPR excitation.[30] Meanwhile, the Tafel slope of A4 is 71 mV/dec is close to that of L4 under 200 mW laser irradiation, proving the maintained OER performance after 5-min treatment of 200 mw laser irradiation.

Figure 4a exhibits the X-ray photoelectron spectroscopy (XPS) spectra of Au-MnO_2 catalysts with and without laser irradiation, where an obvious energy gap exists. The electron binding energy of Mn 3s in Au-MnO_2 catalysts increases by 0.3 eV after 5-min exposure of 200 mW 532 nm laser irradiation. Meanwhile, the electron binding energy spectra of Mn 2p were almost unaltered as shown in Figure S4 [SI]. To further examine this plasmonic effect, electron paramagnetic resonance (EPR) spectra of Au-MnO_2 nanocomposites were measured with and without laser irradiation (200 mW, 532 nm). As reference, pure MnO_2 nanosheets were also tested. As shown in Figure 4b and Figure S7 [SI], loading of GNSs does not lead to any detectable difference of the EPR signals, whereas the induce of 532 nm laser to Au-MnO_2 nanocomposites causes an obvious signal alteration at 1582 Gs in comparison to the dark environment. These results clearly indicate the formation of active Mn^{n+}, in which the outer electrons are somehow confined by LSPR; and demonstrate that the generation of "hot holes" on gold surface by LSPR excitation is capable of confining the outer electrons of Mn cations and promotes the electron transfer from δ-MnO_2 to gold.

To elucidate the OER charge transfer process, electrochemical impedance spectroscopy (EIS) Nyquist plots of Au-MnO_2 hybrids measured with and without 532 nm laser irradiation were performed at 1.65 V (vs RHE), as shown in **Figure 5**a. All impedance spectra are fitted using an equivalent RC circuit model, which consists of a resistor (R_s) and a charge transfer resistance (R_{ct}).[37] R_s and R_{ct} represent the resistivity of the electrolyte between the working and reference electrodes and the charge transfer resistivity of Au-MnO_2 hybrids, respectively. The R_{ct} of Au-MnO_2 hybrids is 180 Ω under 200 mW 532 nm laser irradiation, which is much lower than that of the same sample under dark environment (275 Ω). This result also indicates

that the plasmon excited "hot holes" cause a higher charge transport efficiency in the electrode and the catalysts under 532 nm laser irradiation is more kinetically favorable.

Based on the aforementioned results, we propose the following possible mechanism to be responsible for the generation of active Mn^{n+} species and subsequent improvement on OER catalysis over the Au-MnO_2 hybrid catalysts under 532 nm laser irradiation, as shown in Figure 5b. Under the 532 nm laser irradiation, plasmonic "hot holes" on the gold surface are generated as the effective electron traps to confine the outer electron of Mn^{4+} since the plasmonic "hot electrons" are transferred to the electrode with the assistance of an external voltage.[38,39] Then, the formation of electron-confined active Mn^{n+} species would provide active sites to extract electrons from OH^-, facilitating the formation and subsequent deprotonation of the key OOH intermediates and finally giving rise to the O_2 evolution.[16,18,19] The strong local field and "hot holes" generated may also help the fast absorbance of OH^- to the active sites of the catalysts. In addition, Figure 5c exhibits the I-t curve of Au-MnO_2 nanocomposite catalysts with periodic laser (532 nm) on and off. It is obvious that removing laser irradiation would lead to an abrupt and remarkable suppression of O_2 evolution. Furthermore, the account for the maintained OER catalytic performance after laser treatment is still unclear and needs further investigation.

3. Conclusion

In this work, we have successfully prepared gold decorated two-dimensional (2D) δ-MnO_2 nanosheets composites with various percentage of gold loading via a simple electrostatic method. The composite showed excellent OER catalytic performance under low power of 200 mW green laser irradiation. The electrochemical results showed that the OER catalytic performance could be severely enhanced by activating the LSPR from GNSs under 532 nm laser irradiation. By tuning the laser intensity from 100 to 200 mW the over-potential is decreased from 0.38 to 0.32 V, which is comparable to IrO_2 and RuO_2 catalysts. Through the

XPS and EPR results, our study indicates that plasmon-induced hot-electron excitation would work as the effective electron trapper to confine the outer electron of Mn^{4+} and lead to the formation of electron-confined active Mn^{n+} species. The active Mn^{n+} species would provide active sites to extract electrons from OH^-, facilitate the formation and the subsequent deprotonation of the key OOH intermediates and finally allow for high efficiency oxygen evolution at lower onset potential. It is believed that our findings may provide insights on the activation of plasmon-promoted electrocatalysis under low power laser irradiation and the design of novel composite electrocatalysts.

Experimental Section

General: All chemical regents were purchased from Sigma-Aldrich and Aladdin and used without any further purification. Double distilled water was used in all experiments.

Synthesis of gold nanospheres: To prepare the gold nanospheres, a CTAB solution (7.5 ml, 0.2 M) was mixed with 2.5 ml of 0.001 M $HAuCl_4$ and the mixture was stirred for 10 min. Then, 0.6 ml of ice-cold 0.01M $NaBH_4$ was added to the mixture, and slowly stirred for another 2 min. The colour of the solution tuned from yellow to brown and then to soft pink in one hour. The solution was kept in room temperature for at 12 h before usage. Double distilled water was used throughout the experiments. After two washes and centrifugation (12000 rpm, 30 min) by double distilled water, the gold colloid was obtained and kept in water solution. As shown in Figure S1 [SI], the resulting particle is 12.9 ± 2.1 nm in diameter with a concentration of 1012 NPs/mL.

Synthesis of δ-MnO_2 nanosheets: To prepare the ultrathin δ-MnO_2 nanosheets, 150 mL of 2 mM $KMnO_4$ was mixed with 40 mL ethyl acetate (99.8 %) in a 250 mL boiling flask under vigorous stirring. The reaction was heated by a water bath at 85 °C for 12 h. Meanwhile, a condenser was utilized to prevent the evaporation of the solvent. This process continued until a

great deal of brownish particles formed, which revealed the end of the reaction. The ultrathin δ-MnO_2 nanosheets could be obtained by centrifugation (4000 rpm, 5 min), washed by double distilled water and ethanol several times to remove the excess potassium permanganate and ethyl acetate. Finally, 15 mL ethanol was added to the centrifuge tube to obtain 10 g/L δ-MnO_2 standard suspension. The SEM images of the "as-prepared" δ-MnO_2 nanosheets are shown in Figure S2.

Preparation of Au-MnO_2 nanocomposites: The Au-MnO_2 nanocomposites were prepared via a self-assembly method. Gold nanospheres were assembled to the δ-MnO_2 nanosheets through the electrostatic interaction. Firstly, 10 mg (1 mL) of δ-MnO_2 were re-dispersed into 10 mL ethanol under vigorous stirring. Then, 4, 6, 8 and 10 ml of "as-prepared" Au colloid solution was added dropwise. After stirring for 3 h and siting for 1 h, the resulting sample Au-δ-MnO_2 nanocomposites were collected as sample 1, 2, 3 and 4, respectively. The concentration of gold loading is 0, 2.3, 4.2, 6.5 and 8.3 wt % based on the calculation, where the sample 0 was the pure δ-MnO_2 without gold loading. In addition, the samples were denoted as L1-L4 under laser irradiation and A1-A4 after the laser irradiation.

Characterizations: SEM was conducted by a Zeiss-Supra55 microscope. HRTEM, SAED and EDS mapping images were recorded on a Tecnai G2 F30 S-TWIN microscope at an acceleration voltage of 300 kV. XRD patterns were examined on a Bruker D8 Advanced X-ray Diffractometer (Cu-Ka radiation: λ = 0.15406 nm). A UV−visible spectrophotometer (Cary 5000, Varian Corp.) was used to measure the absorption spectra of the "as-prepared" samples. The chemical states were measured using an Axis Ultra X-XPS (Kratos Analytical Ltd., UK) equipped with a standard monochromatic Al-K_α source (hv = 1486.6 eV). The surface potentials of the samples dispersed in a water/ethanol (1/1 volume ratio) solution were determined using the Zetasizer Nano ZS-90 system (DLS, Malvern Instruments, England). EPR spectra were recorded on a Bruker A300 electron paramagnetic resonance spectrometer at room temperature.

Electrochemical Measurements: All the electrochemical measurements were carried out in a three-electrode system via a CHI-760E instrument at room temperature. An Hg/HgO (filled with 1 M NaOH aqueous solution) and Pt wire were used as reference and counter electrode, respectively. The working electrode were made by drop-casting 5 μL of sample dispersion (4 mg of catalyst dispersed in 1 mL of 2:1 v/v water/methanol mixed solution containing 60 μL of 5 wt % Nafion) on a glassy carbon (GC, 3 mm diameter) electrode. Linear sweep voltammetry curves were measured at a sweep rate of 5 mV/s. The measured potentials of all the data were converted to the reversible hydrogen electrode (RHE) scale according to the Nernst equation ($E_{RHE} = E_{Hg/HgO} + 0.059 \times pH + 0.098$) scale, and the over-potential (η) at j = 10 mA/cm^2 was determined using the following equation: $\eta = E_{RHE} - 1.23$ V.

Supporting Information

Supporting Information is available from the Wiley Online Library or from the author.

Acknowledgements

This work was supported by the Research Mobility Grant from the Royal Society of Chemistry. The authors acknowledge the technical support from the Testing Center of Yangzhou University. The authors also thank Prof. Catherine J. Murphy at University of Illinois Urbana-Champaign and Prof Huan Pang at Yangzhou University for their helpful discussions.

Received: ((will be filled in by the editorial staff))

Revised: ((will be filled in by the editorial staff))

Published online: ((will be filled in by the editorial staff))

References

[1] J. Zhang, Z. Zhao, Z. Xia, L. Dai, *Nat. Nanotechnol.* **2015**, *10*, 444.

[2] J. Suntivich, K. J. May, H. A. Gasteiger, J. B. Goodenough, Y. Shao-Horn, *Science.* **2011**, *334*, 1383.

[3] M. D. Brown, T. Suteewong, R. S. S. Kumar, V. D'Innocenzo, A. Petrozza, M. M. Lee, U. Wiesner, H. J. Snaith, *Nano Lett.* **2011**, *11*, 438.

[4] P. Gu, M. Zheng, Q. Zhao, X. Xiao, H. Xue, H. Pang, *J. Mater. Chem. A* **2017**, *5*, 7651.

[5] Z. W. Seh, J. Kibsgaard, C. F. Dickens, I. Chorkendorff, J. K. Nørskov, T. F. Jaramillo, *Science.* **2017**, *355*, eaad4998.

[6] P. Gu, Y. Xu, Y. Zhao, W. Liu, H. Xue, H. Pang, *Adv. Mater. Interfaces* **2017**, *4*, 1700589.

[7] M. Zeng, Y. Liu, F. Zhao, K. Nie, N. Han, X. Wang, W. Huang, X. Song, J. Zhong, Y. Li, *Adv. Funct. Mater.* **2016**, *26*, 4397.

[8] L. C. Seitz, C. F. Dickens, K. Nishio, Y. Hikita, J. Montoya, A. Doyle, C. Kirk, A. Vojvodic, H. Y. Hwang, J. K. Norskov, T. F. Jaramillo, *Science.* **2016**, *353*, 1011.

[9] I. Narkeviciute, P. Chakthranont, A. J. M. Mackus, C. Hahn, B. A. Pinaud, S. F. Bent, T. F. Jaramillo, *Nano Lett.* **2016**, *16*, 7565.

[10] M. Favaro, W. S. Drisdell, M. A. Marcus, J. M. Gregoire, E. J. Crumlin, J. A. Haber, J. Yano, *ACS Catal.* **2017**, 1248.

[11] Z. Zhan, Y. Wang, Z. Lin, J. Zhang, F. Huang, *Chem. Commun.* **2011**, *47*, 4517.

[12] J. S. Kim, I. Park, E. Jeong, K. Jin, W. M. Seong, G. Yoon, H. Kim, B. Kim, K. T. Nam, K. Kang, *Adv. Mater.* **2017**, 1606893.

[13] F. Song, K. Schenk, X. Hu, *Energy Environ. Sci.* **2016**, *9*, 473.

[14] Z. Zhuang, W. Sheng, Y. Yan, *Adv. Mater.* **2014**, *26*, 3950.

[15] B. J. Trzes??niewski, O. Diaz-Morales, D. A. Vermaas, A. Longo, W. Bras, M. T. M. Koper, W. A. Smith, *J. Am. Chem. Soc.* **2015**, *137*, 15112.

[16] H. Osgood, S. V. Devaguptapu, H. Xu, J. Cho, G. Wu, *Nano Today* **2016**, *11*, 601.

[17] B. S. Yeo, A. T. Bell, *J. Am. Chem. Soc.* **2011**, *133*, 5587.

[18] M. S. Burke, M. G. Kast, L. Trotochaud, A. M. Smith, S. W. Boettcher, *J. Am. Chem. Soc.* **2015**, *137*, 3638.

[19] L. Trotochaud, S. L. Young, J. K. Ranney, S. W. Boettcher, *J. Am. Chem. Soc.* **2014**, *136*, 6744.

[20] C. Tang, H. S. Wang, H. F. Wang, Q. Zhang, G. L. Tian, J. Q. Nie, F. Wei, *Adv. Mater.* **2015**, *27*, 4516.

[21] K. M. Mayer, J. H. Hafner, *Chem. Rev.* **2011**, *111*, 3828.

[22] P. Gu, D. J. S. Birch, Y. Chen, *Methods Appl. Fluoresc.* **2014**, *2*, 24004.

[23] S. C. Warren, E. Thimsen, *Energy Environ. Sci.* **2012**, *5*, 5133.

[24] K. a Willets, R. P. Van Duyne, *Annu. Rev. Phys. Chem.* **2007**, *58*, 267.

[25] Z. Zhan, F. Grote, Z. Wang, R. Xu, Y. Lei, *Adv. Energy Mater.* **2015**, *5*, 1.

[26] Z. Zhan, R. Xu, Y. Mi, H. Zhao, Y. Lei, *ACS Nano* **2015**, *9*, 4583.

[27] M. A. Noginov, G. Zhu, A. M. Belgrave, R. Bakker, V. M. Shalaev, E. E. Narimanov, S. Stout, E. Herz, T. Suteewong, U. Wiesner, *Nature* **2009**, *460*, 1110.

[28] N. S. Abadeer, M. R. Brennan, W. L. Wilson, C. J. Murphy, *ACS Nano* **2014**, 8392.

[29] T. Ming, H. Chen, R. Jiang, Q. Li, J. Wang, *J. Phys. Chem. Lett.* **2012**, *3*, 191.

[30] G. Liu, P. Li, G. Zhao, X. Wang, J. Kong, H. Liu, H. Zhang, K. Chang, X. Meng, T. Kako, J. Ye, *J. Am. Chem. Soc.* **2016**, *138*, 9128.

[31] Y. Shi, J. Wang, C. Wang, T. T. Zhai, W. J. Bao, J. J. Xu, X. H. Xia, H. Y. Chen, *J. Am. Chem. Soc.* **2015**, *137*, 7365.

[32] S. Wang, Y. Gao, S. Miao, T. Liu, L. Mu, R. Li, F. Fan, C. Li, *J. Am. Chem. Soc.* **2017**, *139*, 11771.

[33] D. K. Smith, B. a Korgel, *Langmuir* **2008**, *24*, 644.

[34] X. Fan, D. Yang, L. Ding, J. Du, C. Tao, *ChemPhysChem* **2015**, *16*, 176.

[35] L. Liu, S. Ouyang, J. Ye, *Angew. Chemie Int. Ed.* **2013**, *52*, 6689.

[36] W. S. Chang, B. Willingham, L. S. Slaughter, S. Dominguez-Medina, P. Swanglap, S. Link, *Acc. Chem. Res.* **2012**, *45*, 1936.

[37] Z. Shan, P. S. Archana, G. Shen, A. Gupta, M. G. Bakker, S. Pan, *J. Am. Chem. Soc.* **2015**, *137*, 11996.

[38] S. Yu, Y. H. Kim, S. Y. Lee, H. D. Song, J. Yi, *Angew. Chemie Int. Ed.* **2014**, *53*, 11203.

[39] B. Y. Zheng, H. Zhao, A. Manjavacas, M. McClain, P. Nordlander, N. J. Halas, *Nat. Commun.* **2015**, *6*, 1.

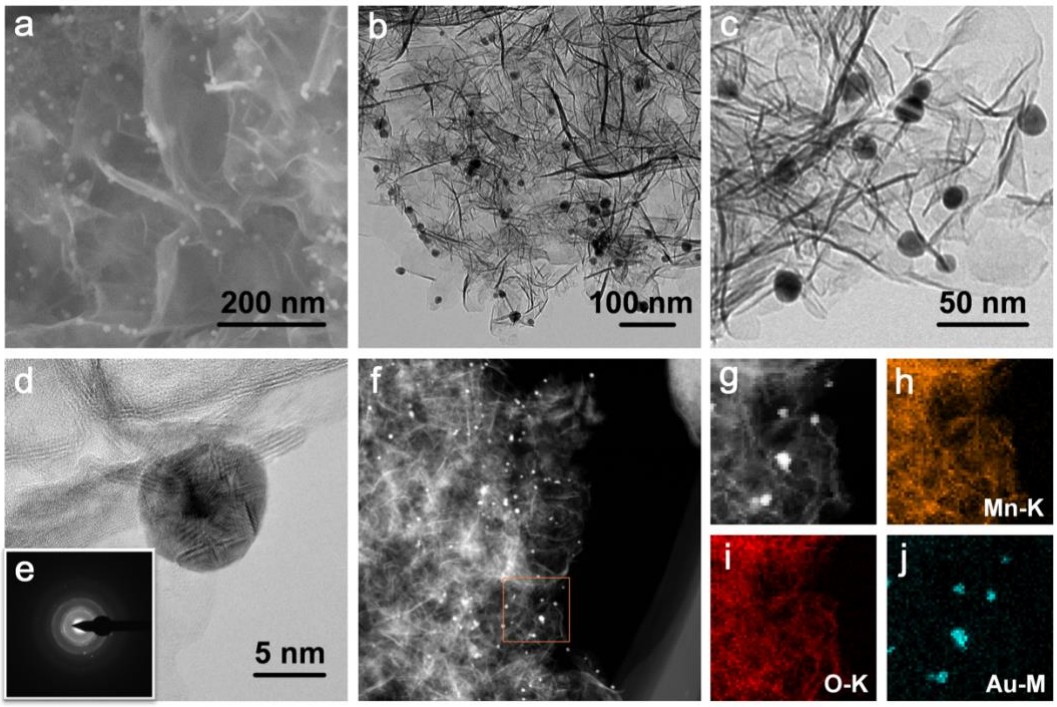

Figure 1. (a) SEM, (b, c) TEM and (d) high resolution TEM images of the Au-MnO_2 nanocomposites; the inset (e) shows the corresponding SAED pattern. (f) STEM image of the Au-MnO_2 nanocomposites; (g-j) STEM image and 2D element mapping images of Mn, O and Au in the area shown in (f), respectively.

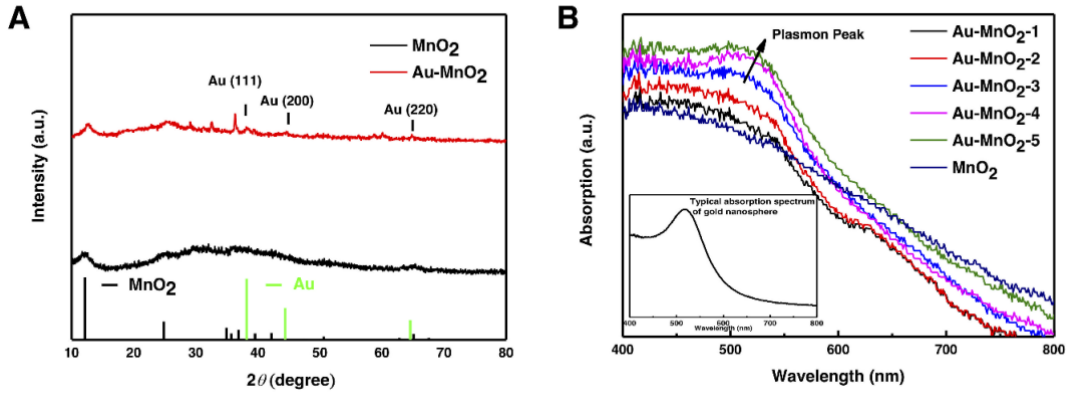

Figure 2. (a) XRD patterns of the MnO_2 nanosheets and Au-MnO_2 nanocomposites; (b) absorption spectra of MnO_2 nanosheets and Au-MnO_2 nanocomposites with various Au loading concentrations. The inset shows a typical surface plasmon peak of GNSs.

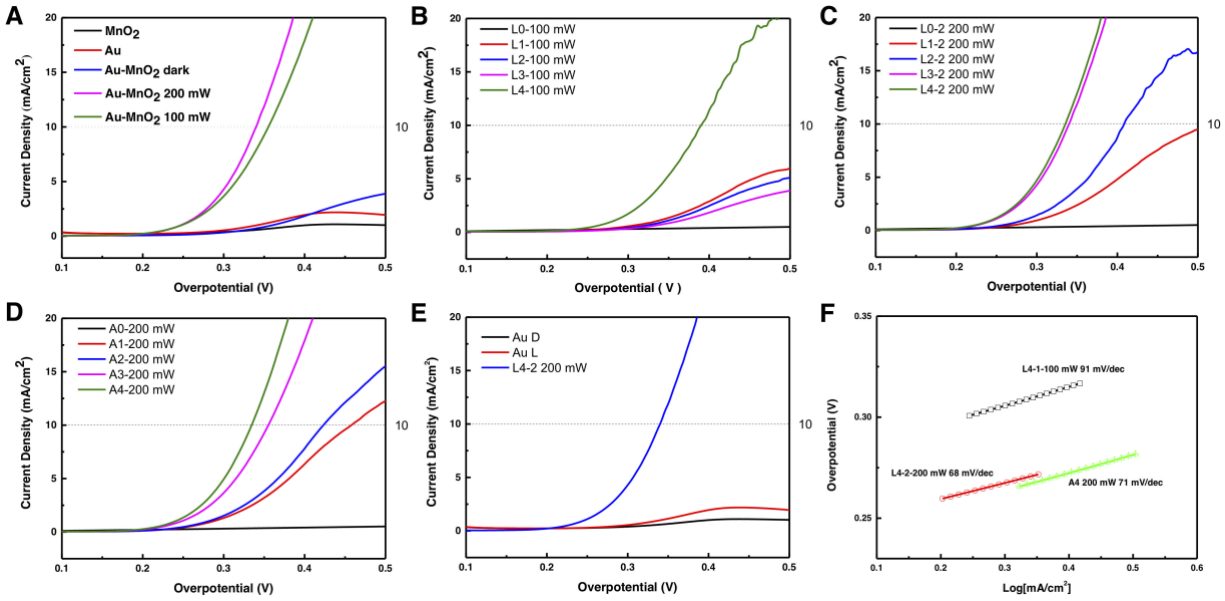

Figure 3. Electrochemical performance of the Au-MnO_2 nanocomposites in 0.1 M KOH electrolyte with and without 532 nm laser irradiation. (a-e) OER polarization curves at the scan rate of 5 mV/s of different samples under various conditions (dark, 100, 200 and after 200 mW laser treatment); (f) Tafel plots of the Au-MnO_2 catalysts under 100, 200 and after 200 mW laser treatment.

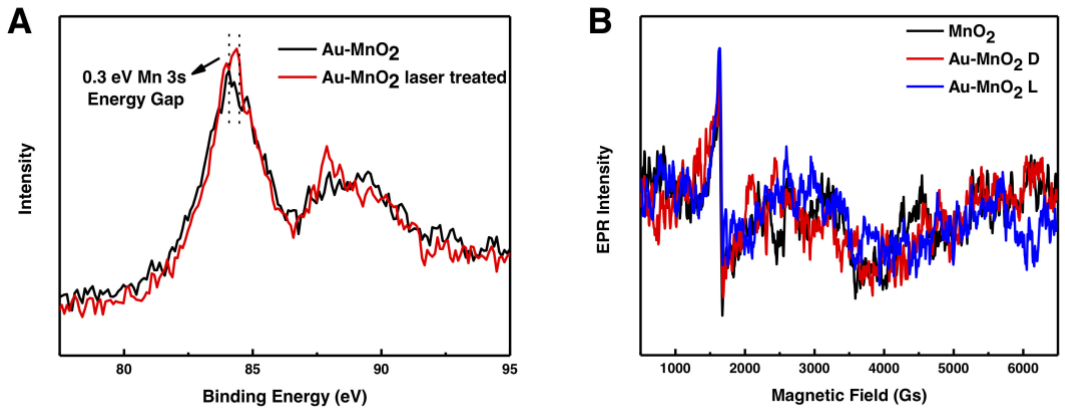

Figure 4. (a) High resolution Mn 3s XPS spectra of the Au-MnO_2 nanocomposites with and without 532 nm laser irradiation process. (b) Electron paramagnetic resonance (EPR) spectra of Au-MnO_2 nanocomposite in solution.

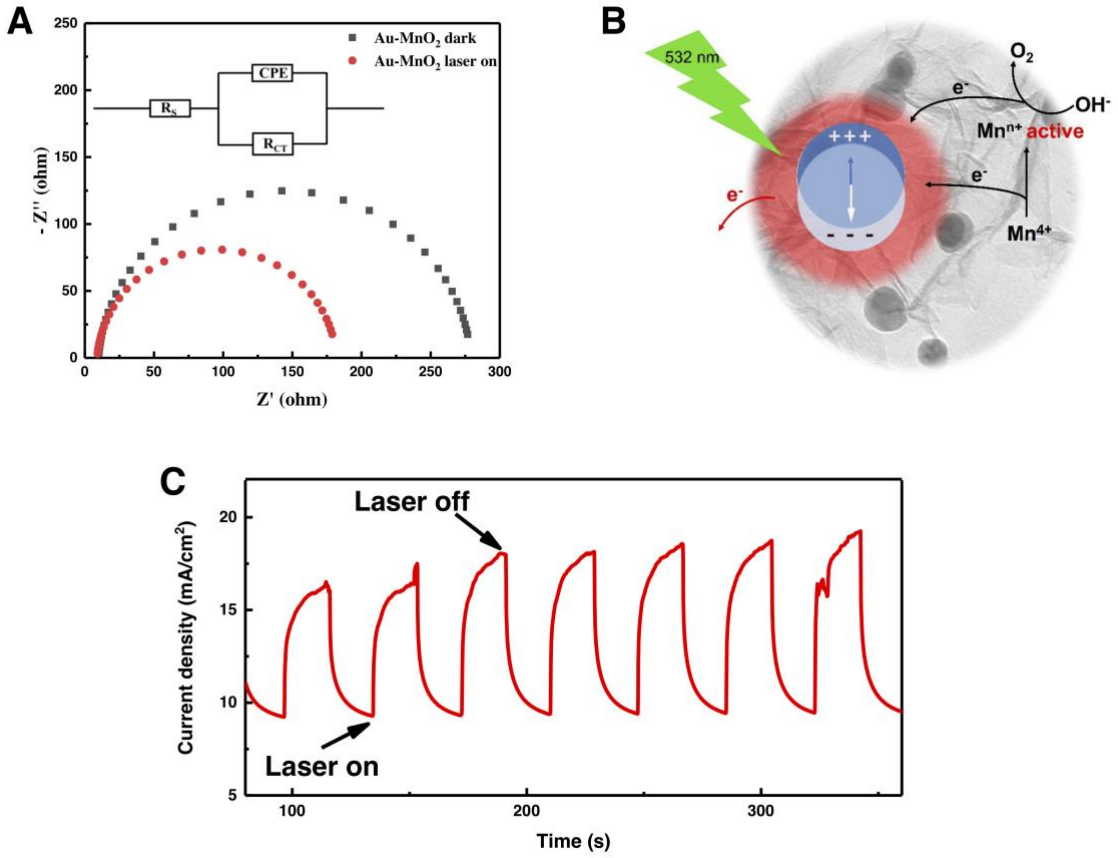

Figure 5. (a) Electrochemical impedance spectroscopy (EIS) Nyquist plots of Au-MnO_2 hybrids measured with and without 532 nm laser irradiation. (b) Schematic electron transfer path that possibly occurs in the Au-MnO_2 nanocomposites under 532 nm laser irradiation. (c) Chronoamperomertic I-t curve of Au-MnO_2 nanocomposite catalysts with 532 nm laser on and off.

A plasmon-promoted electrochemical catalyst for oxygen evolution reaction (OER) is developed by integrating gold nanoantennas with MnO_2 nanosheets. This work provides new insights into understanding light-promoted electrochemical OER catalysis, and sheds light on developing new plasmonic electrocatalysts under low power laser or sunlight irradiation.

Keyword surface plasmon resonance, catalysis, hybrid materials, gold nanoparticles, charge transport

Jing Xu, Peng Gu, David J. S. Birch and Yu Chen**

Plasmon-Promoted Electrochemical Oxygen Evolution Catalysis from Gold Decorated MnO_2 Nanosheets under Green Light

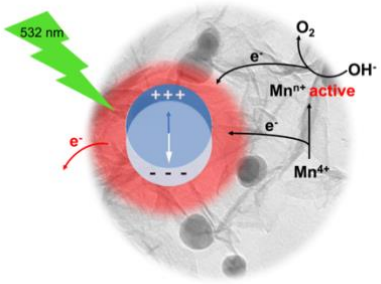

Supporting Information

Plasmon-Promoted Electrochemical Oxygen Evolution Catalysis from Gold Decorated MnO_2 Nanosheets under Green Light

Jing Xu, Peng Gu, David J. S. Birch and Yu Chen**

J. Xu, Dr. P. Gu
Department of Chemistry, Fudan University, 2005 Songhu Road, Yangpu District, Shanghai 200438, P. R. China
E-mail: tommy861007@hotmail.com
Dr. P. Gu, Prof. D. J. S. Birch, Prof. Y. Chen
Photophysics Group, Department of Physics, SUPA, University of Strathclyde, 107 Rottenrow, Glasgow G4 0NG, UK
E-mail: y.chen@strath.ac.uk
J. Xu, Dr. P. Gu
School of Chemistry and Chemical Engineering, Yangzhou University, 180 Siwangting Road, Yangzhou, Jiangsu Province 225002, P.R. China

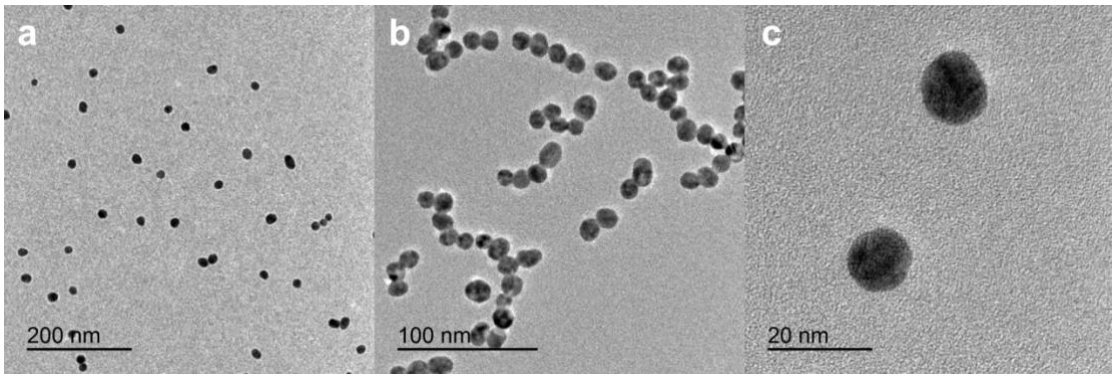

Figure S1. TEM images of gold nanospheres on (a) 200 nm, (b) 100 nm and (c) 20 nm scale.

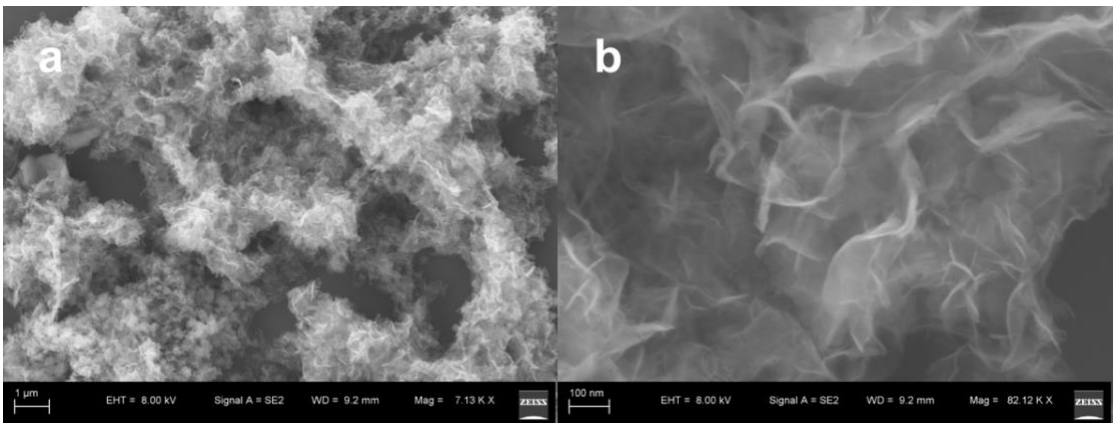

Figure S2. SEM images of 2D δ-MnO_2 nanosheets on (a) 1000 nm and (b) 100 nm scale.

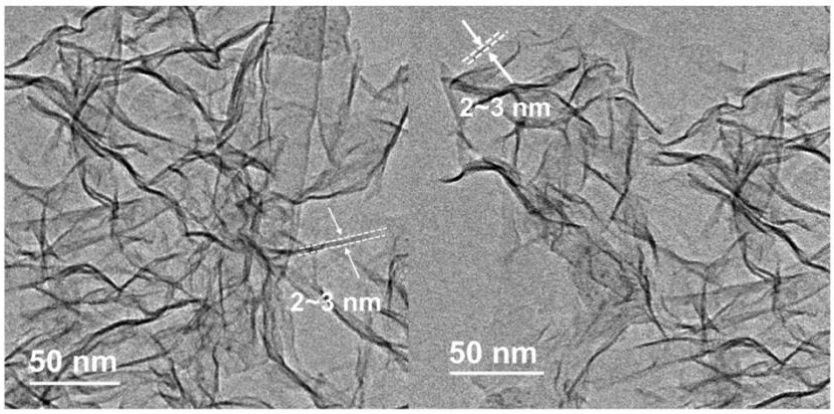

Figure S3. TEM images of 2D δ-MnO_2 nanosheets on 50 nm scale.

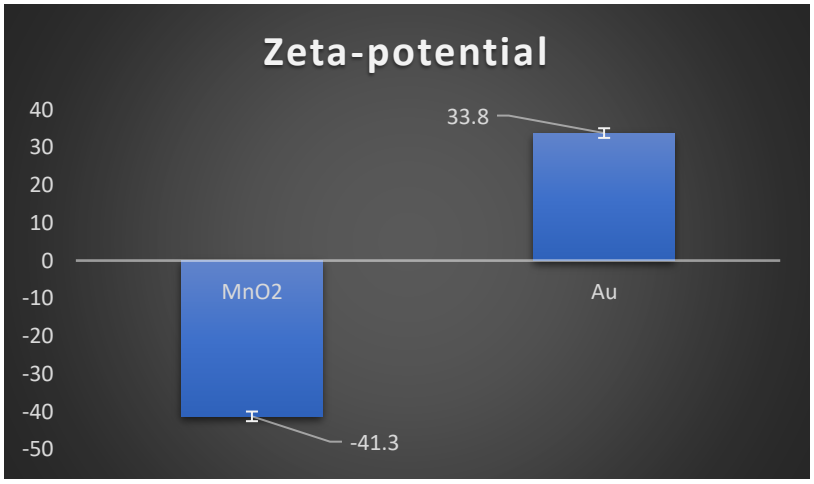

Figure S4. Zeta-potentials of MnO_2 nanosheets and gold nanoparticles well dispersed in water/ethanol (2:3 volume ratio) mixture.

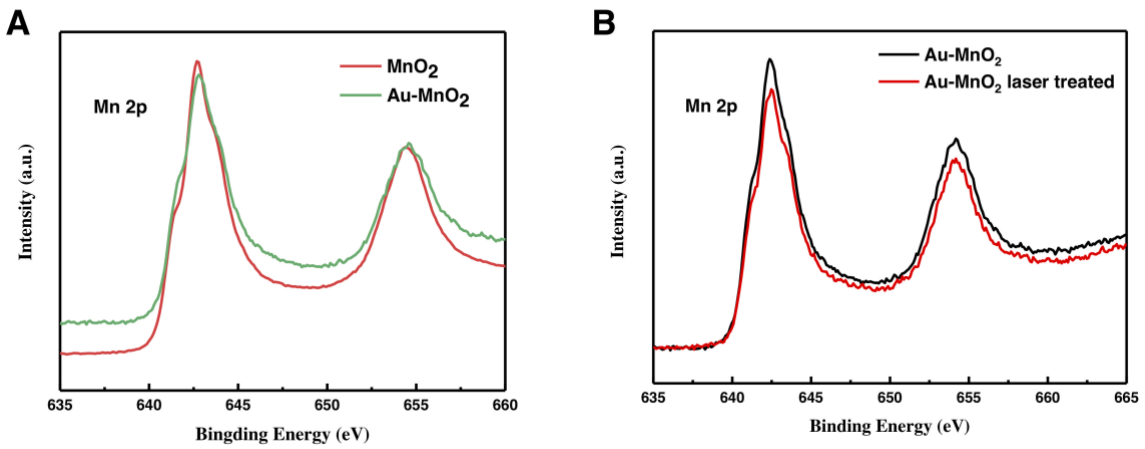

Figure S5. (a) High resolution Mn 2p XPS spectra of MnO_2 and Au-MnO_2. (b) High resolution Mn 2p XPS spectra of the Au-MnO_2 nanocomposites with/without 532 nm laser irradiation.

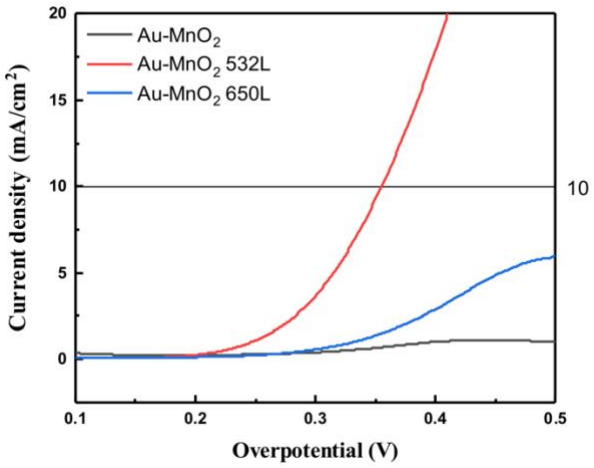

Figure S6. OER polarization curves at the scan rate of the 5 mV/s of Au-MnO_2 nanocomposite catalysts in 0.1 M KOH electrolyte under dark, 532 nm and 650 nm laser irradiation.

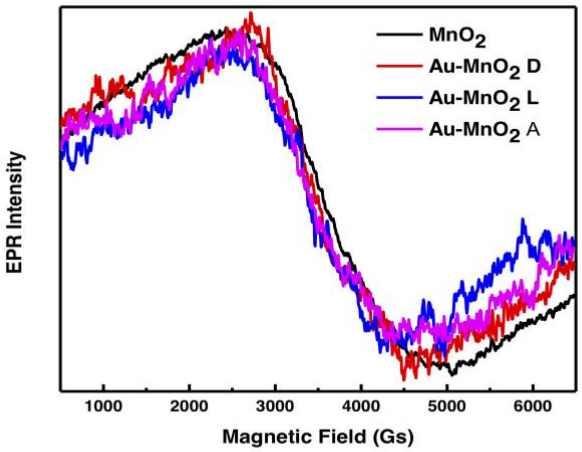

Figure S7. EPR spectra of "as-prepared" dried samples under dark and 532 nm laser irradiation.

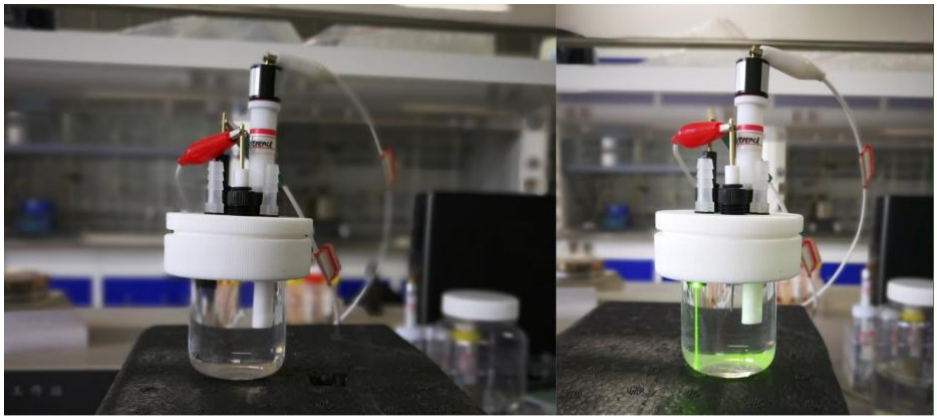

Figure S8. The setup of OER catalysis measurements with light off and on.